Structure
Article

# Structural Insight into the *Mycobacterium tuberculosis* Rv0020c Protein and Its Interaction with the PknB Kinase

Christian Roumestand,[1,2,3] Jade Leiba,[4] Nathalie Galophe,[1,2,3] Emmanuel Margeat,[1,2,3] André Padilla,[1,2,3] Yannick Bessin,[1,2,3] Philippe Barthe,[1,2,3] Virginie Molle,[4] and Martin Cohen-Gonsaud[1,2,3,*]
[1]CNRS UMR 5048, Centre de Biochimie Structurale, 29, rue de Navacelles 34090 Montpellier, France
[2]INSERM U1054, 34090 Montpellier, France
[3]Université Montpellier I et II, Montpellier, France
[4]Laboratoire de Dynamique des Interactions Membranaires Normales et Pathologiques, Universités de Montpellier II et I, CNRS UMR 5235, case 107, Place Eugène Bataillon, 34095 Montpellier Cedex 05, France
*Correspondence: martin@cbs.cnrs.fr
DOI 10.1016/j.str.2011.07.011

## SUMMARY

**The protein Rv0020c from *Mycobacterium tuberculosis*, also called FhaA, is one of the major substrates of the essential Ser/Thr protein kinase (STPK) PknB. The protein is composed of three domains and is phosphorylated on a unique site in its N terminus. We solved the solution structure of both N- and C-terminal domains and demonstrated that the approximately 300 amino acids of the intermediate domain are not folded. We present evidence that the FHA, a phosphospecific binding domain, of Rv0020c does not interact with the phosphorylated catalytic domains of PknB, but with the phosphorylated juxtamembrane domain that links the catalytic domain to the mycobacterial membrane. We also demonstrated that the degree and the pattern of phosphorylation of this juxtamembrane domain modulates the affinity of the substrate (Rv0020c) toward its kinase (PknB).**

## INTRODUCTION

The eukaryotic-like Ser/Thr protein kinases (STPKs) control numerous pathways in *Mycobacterium tuberculosis*, including cell growth initiation, cell division, metabolic flux, or transcription. STPKs substrates linked to novel phosphoregulation pathways are continuously discovered (Alber, 2009; Molle and Kremer, 2010). Among the numerous substrates identified for the 11 *M. tuberculosis* STPKs, a family can be defined by the presence of a approximately 80 amino acids ForkHead Associated (FHA) domain. The FHA domain is a phosphopeptide-specific binding domain found in bacteria, yeasts, plants, or mammalians, able to specifically bind to sequences containing phosphothreonine (Mahajan et al., 2008). In *M. tuberculosis*, five FHA-containing proteins are present with no apparent functional link, all of them being STPKs substrates. The first mycobacterial FHA-containing protein identified was the protein EmbR (Alderwick et al., 2006), a transcriptional regulator involved in regulating arabinogalactan biosynthesis, which DNA binding activity is modulated by PknH phosphorylation (Molle et al., 2003). Rv1747 is an ABC transporter, which is necessary for growth of *M. tuberculosis* in vivo and contains two FHA domains being specifically recognized by the mycobacterial kinase PknF (Curry et al., 2005; Molle et al., 2004). Experiments to determine how PknF regulates the function of Rv1747 demonstrated that phosphorylation occurs on two specific threonine residues, and positively modulates Rv1747 function in vivo via its FHA-1 domain (V. Molle, unpublished data). GarA (Rv1827) is a TCA regulator. It has been shown that the unfolded N-terminal extension of the FHA domain is phosphorylated on two different sites by either PknG or PknB and that phosphorylation promotes the inhibition of the protein and releases the repression of the glutamate dehydrogenase, the α-ketoglutarate decarboxylase and a subunit of the glutamine synthetase, three major TCA enzymes (O'Hare et al., 2008). The two last members of this FHA-family are Rv0020c and Rv0019c, also called FhaA and FhaB, respectively. Their functions remain unknown, but their corresponding genes are located upstream of the kinases *pknB* (*rv0014c*) and *pknA* (*rv0015c*), the penicillin binding protein *pbpA* (*rv0016c*), the cell division protein *rodA* (*rv0017c*), and the Ser/Thr phosphatase *ppp* (*rv0018c*) genes. As a consequence, it has been postulated that the function of Rv0020c and Rv0019c may be linked to the cell wall biosynthesis and/or its regulation (Fernandez et al., 2006). This hypothesis has been strengthened in a recent study proposing that Rv0019c could regulate PapA5, a protein involved in phthiocerol dimycocerosate biosynthesis (Gupta et al., 2009). However, the mode of action at a molecular level remains to be elucidated. The domain architecture of this protein is supposed to be similar to GarA (V. Molle, unpublished data). Rv0020c is a larger protein (527 aa), with a C-terminal FHA domain linked to a approximately 130 amino acids N-terminal domain of unknown function by a 300 residues Pro/Gly rich intermediate domain. No functional data are available on Rv0020c, and no precise function has been proposed.

In this study, we first solved the solution structure of both Rv0020c N-terminal and C-terminal domains by NMR. We showed that the intermediate domain is unfolded and that the N- and C-terminal domains behave independently. We determined the phosphorylation site of Rv0020c and demonstrated that the phosphorylation does not induce any structural

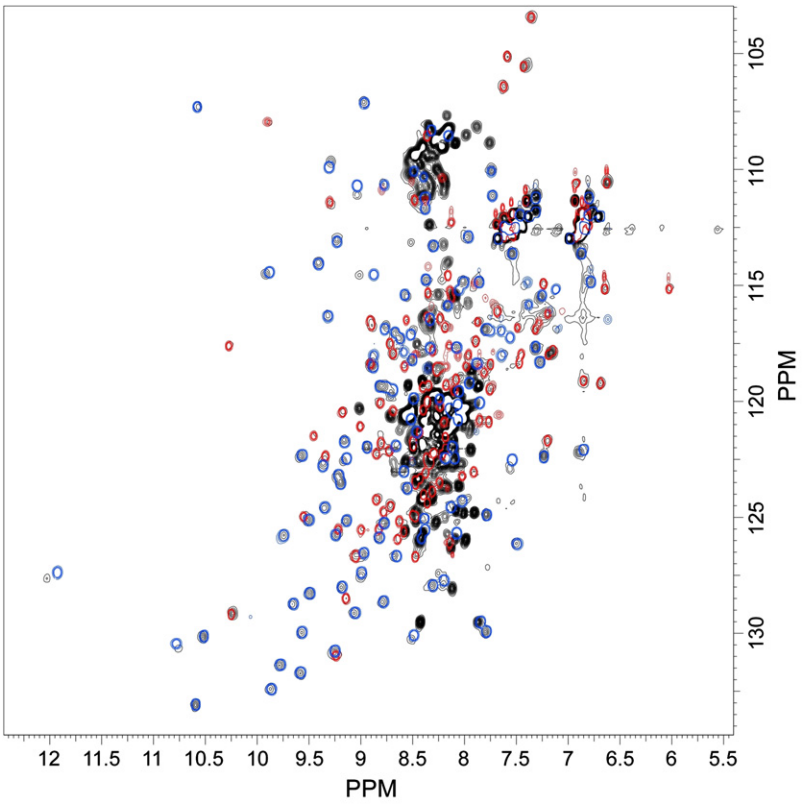


**Figure 1. Superimposition of the [$^1$H,$^{15}$N] HSQC Spectra of Full-Length, N-Terminal, and C-Terminal Domains of Rv0020c**

Superimposition of the [$^1$H,$^{15}$N] HSQC spectra obtained at 700 MHz (pH 6.8 and 20°C), of Rv0020c full-length (black), Rv0020c_FHA (blue), and Rv0020c_Nter (red). The averaged chemical shift differences ($\Delta\delta$) as a function of the protein sequence are given in Figure S1. See also Figure S2.

changes as observed for GarA (Barthe et al., 2009; Nott et al., 2009), linked to an autoinhibition mechanism. Furthermore, we investigated the interaction between Rv0020c and the kinase PknB. We showed that the FHA domain of Rv0020c binds with high affinity to the phosphorylated PknB, and that this interaction involves the STPK juxtamembrane domain and not the catalytic domain itself. Finally, we presented evidences of affinity modulation dependent of the phosphorylation pattern of the PknB juxtamembrane domain, suggesting that a phosphorylation site was predominant. These complex interactions between the FHA substrate and its kinase illustrate the elaborate phosphoregulation network in *M. tuberculosis* and bring new features into the function of FHA containing STPKs substrates.

## RESULTS AND DISCUSSION

### Domain Delimitation

Bioinformatics studies using different web-based servers allowed us to identify the approximately 95 residues FHA domain (residues 430–527) within the 527 amino acid sequence of Rv0020c. From multiple-sequence analysis and hydrophobic cluster analysis (Callebaut et al., 1997), an N-terminal domain (residues 1–132) emerges with no apparent similarities with known proteins. In between these two domains (residues 133–429), the protein possesses a 300 amino acids PG-rich ''domain'' (proline: 17.2%; glycine: 23.2%), with a very low content in hydrophobic residues (Ile+Leu+Met+Phe+Trp+Val: 3%) except for the tyrosine (13.6%). The low content in hydrophobic residues of this intermediate domain allowed us to define precisely its delimitations. Direct Rv0020c homologs, with homologous sequences for both N-ter and Cter domains, exist for closely related organisms. Noteworthy some of these proteins lack the intermediate PG-rich domain and only possess the N-terminal and the FHA domain, while some close homolog have a slightly shorter intermediate PG-rich domain (20 residues shorter in *M. avium* and 50 residues for *M. leprae*). To initiate the structural and interaction studies we cloned the N-terminal (Rv0020c_Nter) and the FHA (Rv0020c_FHA) domain separately in addition to the full-length protein.

### The Structure of the N- and C-terminal Domains Are Similar in the Isolated or in the Full-Length Proteins

Confirming the bioinformatic analysis, the spectra of Rv0020c-Nter and Rv0020c_FHA form complementary subsets of the spectrum from full-length Rv0020c (Figure 1): cross-peaks in the [$^1$H,$^{15}$N] HSQC spectra of each isolated domain protein overlap with a cross-peak in the [$^1$H,$^{15}$N] HSQC spectrum of the full-length protein, showing only weak chemical shift variations that concern essentially the C-terminal FHA domain (see Figure S1 available online). This suggests that residues from the N- and C-terminal domain are in a similar environment either in the full-length construct or in an isolated domain, supporting that the Nter and FHA domains constitute independently folded modules, without any interaction between the two domains. Moreover, the resonance line widths measured in the three spectra for the N- and C-terminal domains are very similar, further indicating that these domains are significantly dynamically decoupled. The others residues, corresponding to the 133–429 PG-rich peptidic segment, gave rise to the intense cross-peaks centered at 8.5 ppm in the proton dimension of the [$^1$H,$^{15}$N] HSQC spectrum of the full-length protein, thus strongly suggesting that this segment adopts a random-coil conformation. From these observations, we decided to solve the solution structure of the N- and C-terminal domain of Rv0020c independently.

### NMR Structures of the N-Terminal and the C-Terminal Domains

The assigned [$^1$H,$^{15}$N] HSQC spectrum of Rv0020c_Nter and Rv0020c_FHA are shown in Figure S2. By combining the information from the double- and triple-resonance heteronuclear experiments, we were able to assign 94.5% and 99% of the amide group resonances for the nonproline residues (four and two prolines), 92.9% and 100% of the other backbone

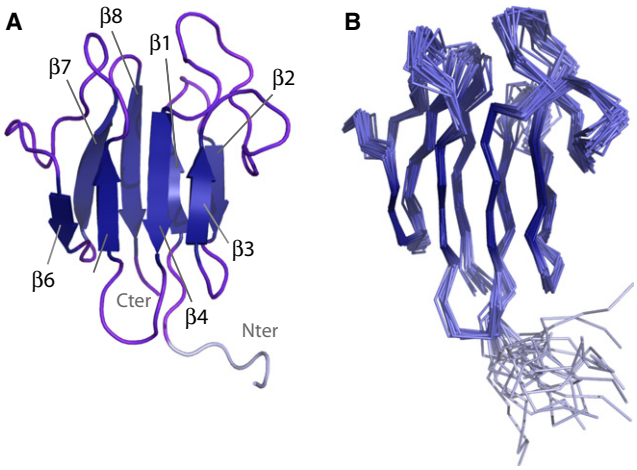


**Figure 2. Cartoon Representation of the Rv0020c_FHA Structure**
(A) The N-terminal part of the protein from Gly430 to Gly433 is disordered and represented in gray.
(B) Representation of the final ensemble of 30 NMR structures of Rv0020c_FHA.

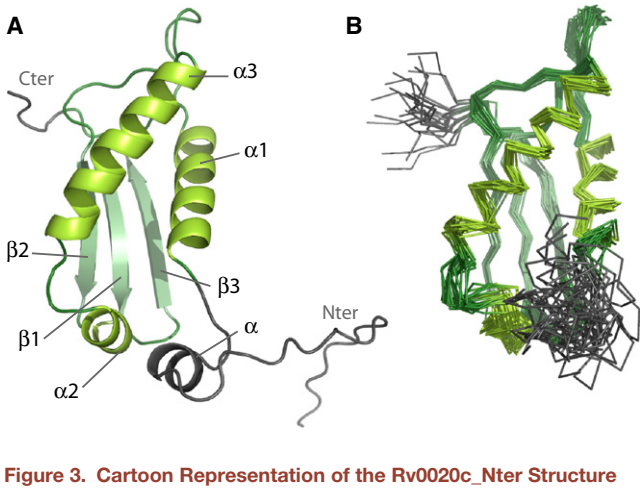


**Figure 3. Cartoon Representation of the Rv0020c_Nter Structure**
(A) The N-terminal part of the protein from Met1 to Val32 is disordered and represented in gray.
(B) Representation of the final ensemble of 30 NMR structures of Rv0020c_Nter. See also Figure S3.

resonances (Cα, C' and Hα), 85.7% and 100% of the Cβ resonances, and 84.1% and 94.4% of the side-chain protons for Rv0020c_Nter and Rv0020c_FHA, respectively. The chemical shift table was deposited in the BMRB databank (accession numbers 17585 and 17586 for Rv0020c_Nter and Rv0020c_FHA, respectively).

CYANA calculations performed for the C-terminal domain of Rv0020c revealed a well-defined FHA domain. The global fold of the FHA domain, a β sandwich composed of 11 strands, is well conserved (Figure 2) and similar to the recently X-ray structure (PDB 3PO8) determined for the same domain (root-mean-square deviation [rmsd] of 1.5 Å) (Pennell et al., 2010). In the case of the N-terminal domain, the calculation yields a less canonical structure: the domain folds into a globular structure, encompassing a triple stranded β sheet flanked on one side by two amphipatic α helices (α1, α3), with a topology of α1β3α3β1β2 (Figure 3). Helix 1 (Pro33-Asp46) and helix 3 (Glu79-Glu95) adopt a parallel disposition, with an angle of around 45° relative to each other. Strand β2 (Val105-Gln110) is oriented parallel to β1 (Glu61-Leu66), while β3 (Arg120-Gly123) is antiparallel to β1. This αβ sandwich is stabilized by numerous hydrophobic contacts between helix 1 and 3 and the hydrophobic face of the triple stranded β sheet. A third short helix α2 (Val68-Leu74) caps one extremity of this αβ sandwich. Consistent with the absence of long-range NOEs, the 32 first residues adopt a random-coil conformation, with the exception of residues Ala22 to Phe27 that form a short dynamic helix, essentially defined by TALOS restraints. The coordinates have been deposited in the PDB: 2LC0 for the N-terminal domain and 2LC1 for the FHA C-terminal domain of Rv0020c.

The DALI (Holm and Rosenström, 2010) and SSM (Krissinel and Henrick, 2004) servers were used to find possible structural homologs for Rv0020c_Nter. The best and only reliable result corresponds to the HypA protein from *Helicobacter pylori*, a putative metallochaperone for the [NiFe] hydrogenase maturation (PDB 2KDX, Figure S3). This protein is a weak $Ni^{2+}$ and strong $Zn^{2+}$ binding protein (Xia et al., 2009). The structural conservation is only engulfing the core of the secondary structure composed by the α helices α1, α3 and the β strands, β1, β2, and β3 (rmsd of 3.2 Å for 80 aa). The α helix α2 located between the β1 and α3 is absent in HypA. Also, the α1/β1 (residues 48–58) and α3/β3 (residues 97–104) loops are longer in Rv0020c_Nter. The accessory $Zn^{2+}$ binding domain of HypA is missing in the Rv0020c_Nter domain, replaced by a short loop between the β strand β2 and β3 (Rv0020c_Nter numbering). The low affinity binding site for $Ni^{2+}$ was characterized and is composed of the residues His2, Glu3, and Asp40 in HypA. While the equivalent Glu is present in Rv0020c_Nter, the two other residues at equivalent positions are neither conserved nor homologous. Thus, after examination of these two related domains, no related functional property could be deduced from the comparison between the proteins Rv00020c and HypA. Consequently, only based on the structure knowledge, no conclusion could be drawn on the putative function of the Rv0020c N-terminal domain.

## Rv0020c Is Phosphorylated at a Unique Threonine Residue

Recombinant Rv0020c protein was incubated with cold ATP in the presence of PknB, and subjected to mass spectrometry analysis after tryptic digestion. ProteinPilot database searching software (version 2.0, Applied Biosystems), using the Paragon method with phosphorylation emphasis, was used to detect and identify the phosphorylated peptides. The sequence coverage of the protein was 97% and phosphorylation occurred only on peptide [108–120]. The MS/MS spectrum of the corresponding triple charged ion at m/z 544.2 unambiguously confirmed the presence of the phosphate group on the threonine residue Thr116 (Figure S4). Definitive identification and localization of Thr116 as being the unique phosphorylation site in Rv0020c was achieved by site-directed mutagenesis to introduce a mutation that prevents specific phosphorylation (Thr116 to Ala116 replacement). This mutant was expressed, purified, and used in an in vitro kinase assay. The recombinant

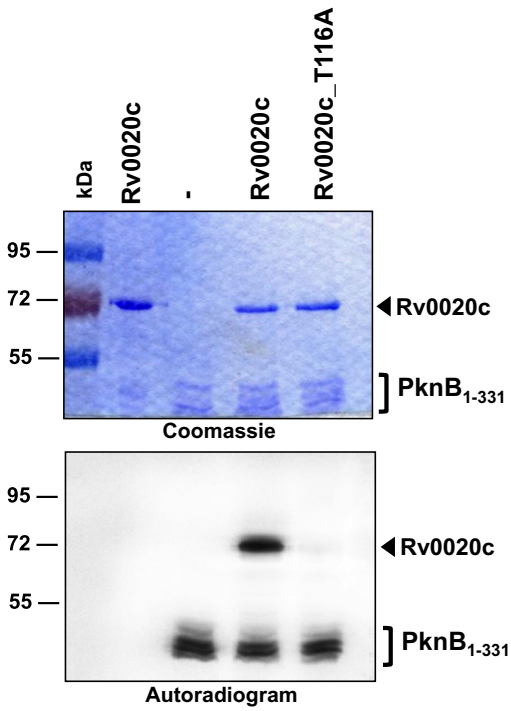


**Figure 4. In Vitro Phosphorylation of the Rv0020c Derivatives by PknB_331**

Purified Rv0020c_WT and Rv0020c_T116A were incubated with PknB_331 and [$\gamma$-$^{33}$]ATP. Samples were separated by SDS-PAGE, stained with Coomassie blue (upper panel) and visualized by autoradiography (lower panel) after overnight exposure to a film, as indicated. Upper bands reflect the autophosphorylation activity of Rv0020c and the lower bands correspond to the autophosphorylation signal of PknB_331. See also Figures S4 and S5.

Rv00020c_T116A was incubated along with [$\gamma$-$^{33}$P]ATP and PknB. The mixture was separated by SDS-PAGE and analyzed by autoradiography. As shown in Figure 4 (upper panel), equal amounts of Rv0020c_WT or mutant Rv00020c_T116A were used. Phosphorylation of Rv0020c_T116A was completely abrogated, compared with phosphorylation of Rv0020c_WT, as evidenced by the absence of a specific radioactive band (Figure 4, lower panel). These results unambiguously demonstrate that Rv00020c_T116A has lost its ability to be phosphorylated by PknB. Moreover, an additional round of mass spectrometry analysis was performed on Rv00020c_T116A pretreated with cold ATP and PknB, which failed to identify any additional phosphate group that could eventually have arisen as a compensatory mechanism due to the loss of the Thr116 phosphorylation (data not shown). Noteworthy, the phosphorylation site is located in the short loop between the $\beta$ strand $\beta$2 and $\beta$3, where the accessory $Zn^{2+}$ binding domain is found in HypA (see above).

## No Interaction Detected between the Phosphorylated N-Terminal Domain and the FHA C-Terminal Domain

The modular organization of Rv0020c with a phosphorylated N-terminal domain and a C-terminal FHA domain linked by a long unfolded segment prompted us to test whether the two domains could bind to each other in a phosphorylation-dependent manner. Such interaction has been shown for GarA and its close homolog OdhI, two others PknB substrates bearing a FHA domain, thus revealing a new autoinhibition mechanism (Barthe et al., 2009; Nott et al., 2009). A [$^{1}$H,$^{15}$N] HSQC spectrum of Rv0020c_Nter was recorded at pH 6.8 at 20°C. The protein was then incubated with PknB, ATP and $Mg^{2+}$ and repurified. A new [$^{1}$H,$^{15}$N] HSQC spectrum of Rv0020c_Nter now phosphorylated (called Rv0020c_Nter_P) was recorded and compared to the one recorded before phosphorylation. In agreement with mass spectrometry, the phosphorylation yields chemical shift variations limited to Thr116 ($\Delta\partial \approx 0.1$ ppm for $^{1}$H, and 0.2 ppm for $^{15}$N), suggesting that the structure of the N-terminal domain remains virtually unchanged upon phosphorylation (Figure S5). Note that, at this pH, chemical shift variations of larger amplitude are expected for the phosphorylated threonine as well as for residues sequentially or spatially close to this residue, due to electrostatic perturbations arising from the negatively charged phosphate group. A closer look to Rv0020c_Nter NMR structure shows that Thr116 side chain is wedged between two imidazole rings of the spatially neighbor residues His69 and His115. This side-chain stacking probably compensates partially for the charge of the phosphate group, thus limiting its electrostatic effects.

The $^{15}$N-labeled sample of Rv0020c_Nter_P was then titrated with increasing amounts of unlabeled Rv0020c_FHA. The final Rv0020c_Nter_P:Rv0020c_FHA ratio tested was 1:5 for an initial concentration of Rv0020c_Nter_P of 50 $\mu$M. Since no chemical shift perturbation upon addition of Rv0020c_FHA (data not shown) was observed, we can conclude that no interaction occurs between the two domains upon phosphorylation of Rv0020c_Nter by PknB, and that the autoinhibition mechanism observed for GarA and OdhI is apparently not similar in the case of Rv0020c.

## Interaction with PknB

While the role of the FHA domain is now partly understood for the GarA protein, the function of this domain in the others FHA containing proteins in *M. tuberculosis* remains elusive. As a phosphospecific binding domain, one hypothesis would be that the FHA domain could promote the substrate recruitment by the STPKs, and especially by PknB, since PknB phosphorylates all the FHA containing proteins (unpublished results). Autophosphorylation patterns are present on the PknB protein sequence, not only in the activation loops but also in the juxtamembrane domain. The two threonines in the activation loop of the catalytic domain (Thr171 and Thr173) are systematically phosphorylated (Durán et al., 2005). As in most of its eukaryotic STPKs homologs, phosphorylation of these residues is essential for PknB activation. In fact, a phosphate group from the activation loop forms an ion pair with a conserved arginine (Arg137 in PknB) located in the catalytic loop of the catalytic domain. This arginine is part of a conserved His-Arg-Asp motif present in eukaryotic STPKs. In addition, the Gly-Thr-Ala motif, necessary for the phosphotransfer between the ATP and the substrate is also conserved in the PknB T-loop (Scheef and Bourne, 2005). These interactions are believed to be critical to obtain the active conformation of the catalytic site (Huse and Kuriyan, 2002). In addition to the two phosphorylation sites, two other systematic phosphorylated residues (Thr294 and Thr309) were identified in the juxtamembrane domain (residues 280–330) linking the

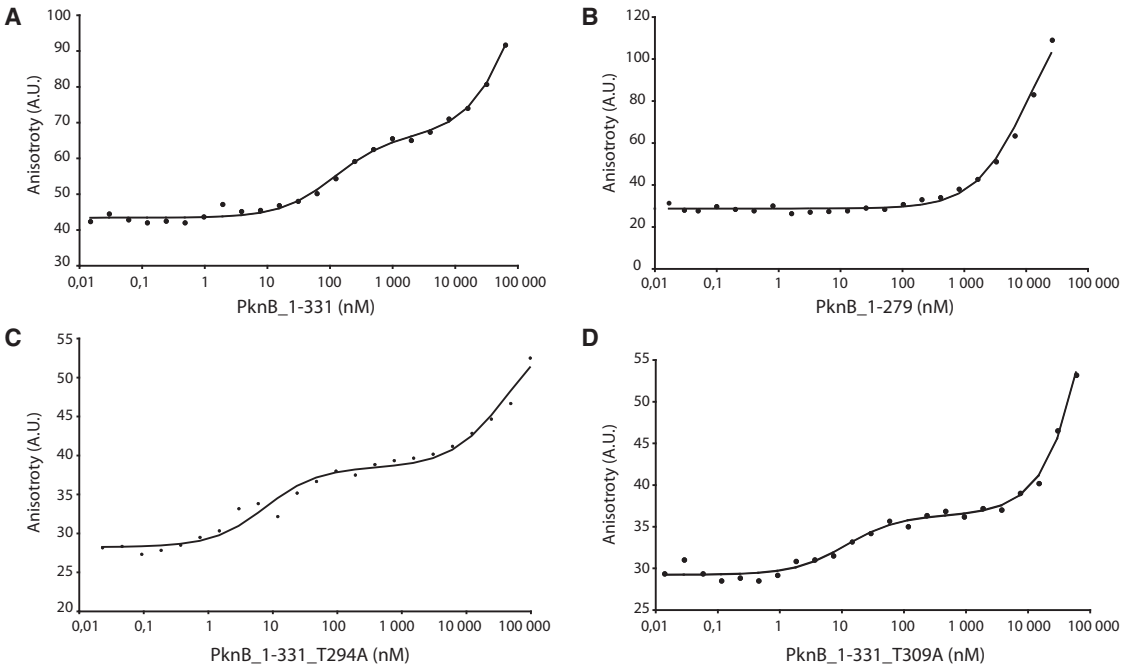


**Figure 5. Fluorescence Anisotropy Binding Profile**

Fluorescence anisotropy binding profile for binding of Atto647N-labeled Rv0020c_FHA (4 nM) with PknB_331 (A), PknB_279 (B), PknB_331_ T294A (C), PknB_331_T309A (D). See also Figure S6.

C-terminal end of the kinase cytoplasmic catalytic domain to the trans-membrane domain (Durán et al., 2005). A similar pattern has also been described in other *M. tuberculosis* STPKs such as PknD, E, and F.

Therefore, the presence of such patterns, in combination with the hypothesis that FHA domains could be involved in the recruitment of substrates by STPKs, led us to investigate the interaction between PknB and Rv0020c.

## The Rv0020-FHA Domain Binds Preferentially to the PknB Juxtamembrane Domain

We first overexpressed two constructions of the PknB kinase. The first construction, PknB_279, is restricted to the sole catalytic domain (residues 1–279) while the second one, PknB_331, corresponds to the catalytic and juxtamembrane domains (residue 1–331). During overexpression in *Escherichia coli*, PknB autophosphorylation occurs, leading to fully phosphorylated samples (Durán et al., 2005). These two proteins were used in fluorescence anisotropy experiments to titrate Rv0020c_FHA protein N-terminally labeled with the Atto647N fluorophore. The binding isotherms presented on Figure 5 were fitted numerically according to a binding model where two PknB proteins bind to Rv0020c_FHA. For PknB_331 (Figure 5A), a Kd value of 110 ± 30 nM could be measured for the high-affinity binding event. As the saturation plateau could not be reached due to PknB instability at high concentration no accurate Kd value could be obtained for the second binding event. Since the concentration of Atto647N-labeled Rv0020c_FHA used for the titration is limiting (4 nM), this second event probably represents the dimerization of PknB_331, which takes place in the micromolar range (our unpublished data). The same experiment was done with PknB_279 and displayed only a weak binding event, which correspond to the binding of Rv0020c_FHA to the catalytic domain of PknB (Figure 5B). These binding experiments demonstrated that juxtamembrane domain is necessary for high affinity FHA binding. The recovered affinity is similar to the one published recently by Pennel et al. measured by isothermal calorimetry between Rv0020c_FHA and a peptide obtained after screening toward an oriented peptide library (Pennell et al., 2010). In order to control whether our measured affinity was not overestimated due to an underestimation of the PknB_331 concentration, we performed a stoichiometric titration where Atto647N-Rv0020c_FHA was present at a concentration (500 nM) well above the Kd for its interaction with PknB_331 (110 ± 30 nM). The binding isotherm (Figure S6) reaches a plateau at one/one [PknB_331]/[Rv0020c_FHA] ratio, indicating that the PknB_331 concentration was not underestimated.

## The Phosphorylation Pattern of the PknB Juxtamembrane Domain Modulates the FHA Binding

As two phosphorylation sites coexist in the juxtamembrane domain of PknB, we investigated whether (1) both sites were involved in the FHA binding, and (2) one was preferential. To do so, we generated two mutant proteins by replacing one of the phosphorylated threonine by an alanine (PknB_331_T294A and PknB_331_T309A), thus suppressing one or the other juxtamembrane phosphorylation site. The two proteins were used in fluorescence anisotropy experiments to titrate Atto647N-labeled Rv0020c_FHA (Figures 5C and 5D). Surprisingly, the two mutant proteins displayed an even higher affinity compared with PknB_331 (10 ± 6 nM and 13 ± 7 nM for PknB_331_T294A and PknB_331_T309A, respectively). To date, these values

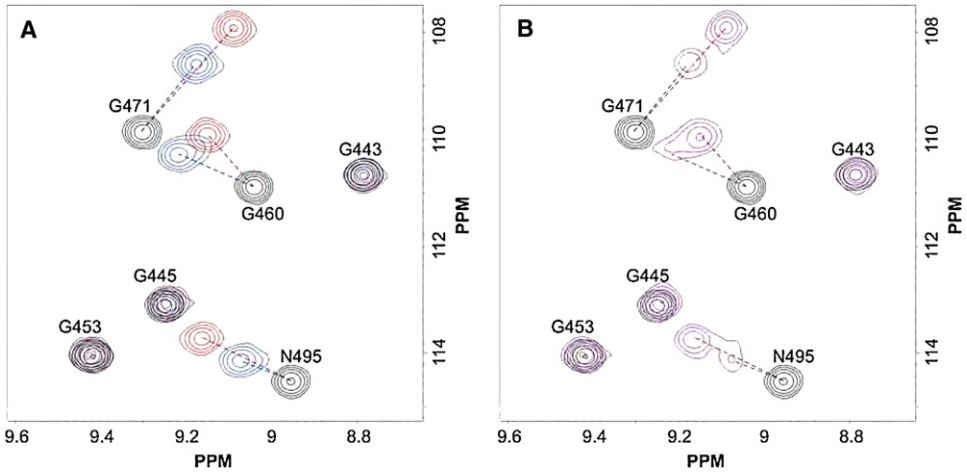


**Figure 6. Superimpositions on Selected of Rv0020c_FHA Alone and in the Presence of Peptides**

Superimpositions of zooms on selected resonances in the full [$^{1}$H,$^{15}$N] HSQC spectra of uniformly labeled samples Rv0020c_FHA (50 μM) alone solution (black) and in the presence of 500 μM concentrations of Pep_294 (red) or Pep_309 (blue) (A), or in the presence of Pep_294/309 (500 μM) (pink) (B). Clearly, the bound Pep_294/309 peptide splits into two unequal populations that occupy two distinct sites at the protein surface. These two sites correspond to the binding sites already found either for Pep_294 (75%, as measured from the relative cross-peak intensity) or for Pep_309 (25%). Spectra were recorded at 500 MHz (20°C and pH 6.8). The corresponding full spectra are presented as Figures S8 and S9. See also Figure S7.

correspond to the highest affinities measured between a FHA domain and its partner.

These results demonstrate that the concomitant phosphorylation of both threonine residues on the PknB juxtamembrane domain is not needed for FHA binding. Moreover, a unique phosphorylation yields a remarkable 10-fold increase in affinity. Possibly, whether a single phosphorylation is needed to promote the binding, a second phosphorylation disturbs this binding. An extra characterization was attempted with the generation of a double mutant, PknB_331_T294A_T309A, in order to assess that phosphorylation is mandatory for the FHA binding. Unfortunately and surprisingly, we were not able to obtain enough of this mutant protein for the fluorescence anisotropy experiments.

## NMR Characterizations of the PknB-Juxtamembrane/Rv0020c-FHA Interaction

In order to understand the FHA domain interaction with the different isoforms of PknB, we synthesized four peptides derived from the juxtamembrane domain of PknB (residues 286–318). The 33 amino acids peptides were either nonphosphorylated (called Pep_NP), phosphorylated on the threonine corresponding to Thr294 (PknB numbering, called Pep_294), phosphorylated on the threonine corresponding to Thr309 (called Pep_309), or phosphorylated on both threonines Thr294 and Thr309 (called Pep_294/309). Each peptide was added to 50 μM samples of $^{15}$N Rv0020c_FHA to final concentrations of 50, 250, and 500 μM respectively, and [$^{1}$H,$^{15}$N] HSQC spectra were recorded.

Addition of Pep_NP did not show any modification in the Rv0020c_FHA [$^{1}$H,$^{15}$N] HSQC spectrum, except for residue Arg474 where a small concentration-dependent drift of the corresponding amide cross-peak was observed (Figure S7A). From the crystal structure of Rv0020c_FHA in complex with a short phosphopeptide published by Pennel et al. (PDB 3POA), arginine 474 participates in long live H-bonds with the phosphate and the carbonyl group of pThr (Pennell et al., 2010). The peptide concentration dependent drift suggests fast exchange conditions between the FHA domain and the unphosphorylated peptide, hence a weak binding (>100 μM). In contrast, the addition of either Pep_294 or Pep_309 changed dramatically the [$^{1}$H,$^{15}$N] HSQC spectrum of Rv0020c_FHA (Figure 6A; Figure S7B), significant chemical shift variations concern amide group in a similar region of the FHA domain, encompassing about 20 residues (Figure 7). The fact that the variations were found to be independent of the peptide concentration indicates a slow exchange between the FHA protein and the peptide, hence a high affinity (<μM). For both peptides, the most affected cross-peaks correspond to residues belonging to the phosphopeptide binding groove. Qualitatively, minor differences exist upon Pep_294 or Pep_309 addition. The most notable variation was observed for residues Thr470 and Gly471, further perturbed when Pep_294 was added ($\Delta\partial$ = 0.17 and 0.29 ppm against 0.13 and 0.18 ppm for Pep_309). Others discrepancies concern residues located on the loop β7/β8 centered on Asn495 ($\Delta\partial$ = 0.23 ppm for Pep_294 against 0.13 ppm for Pep_309). These differences are likely due to local sequence differences between the two peptides, within the segment supporting the phosphothreonine residue directly involved in the interaction with the FHA phosphopeptide binding site.

## The PknB pThr294 Site Corresponds to the Preferential Rv0020c FHA Binding Site

Addition of Pep_294/309, harboring two phosphorylations, to Rv0020c_FHA yields essentially similar perturbations as observed upon addition of Pep_294 (Figure 6B; Figure S7C). A closer look at the HSQC spectrum revealed a second minor population corresponding to the spectrum after addition of Pep_309 (≈25%, as estimated from cross-peak intensities). This suggests that Rv0020C_FHA binds preferentially the peptide segment bearing pThr294, although the Kd measured by

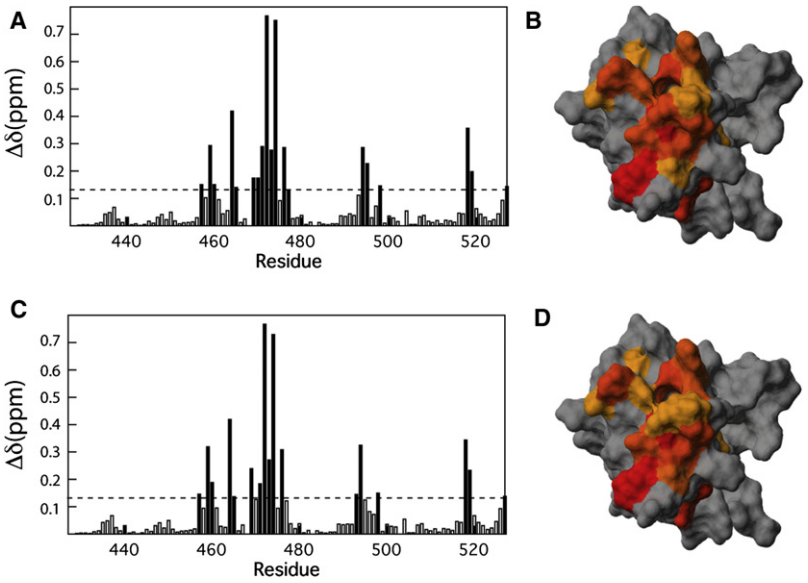


**Figure 7. Amide Averaged Chemical Shift Variations (Δδ) as a Function of the Protein Sequence**

Δδ have been measured between [$^{1}$H,$^{15}$N] HSQC spectra recorded at 500 MHz (20°C and pH 6.8) on 50 μM $^{15}$N-uniformly labeled samples of Rv0020c_FHA before and after addition of 500 μM concentrations of unlabeled peptides Pep_294 (A) or Pep_308 (C), with $\Delta\delta = [\Delta\delta_H^2 + (\Delta\delta_N \cdot \gamma_N/\gamma_H)^2]^{0.5}$. The dotted line stands for the standard deviation (0.13 ppm). The corresponding Van der Waals diagram of the Rv0020c_FHA NMR structure are presented in (B) and (D), with a color gradient indicative of the Δδ value: from gray ($\Delta\delta \approx 0$) to red ($\Delta\delta_{max} > 0.75$ ppm).

fluorescence anisotropy between Rv0020c and PknB_T294A or PknB_T309A were similar.

Taking as a whole, the results from the fluorescence and NMR binding experiments display a complex mechanism of the Rv0020c_FHA binding to PknB_331 with a modulation of the affinity regulated by the site and the degree of phosphorylation of the juxtamembrane domain.

## Conclusion

The FHA-containing proteins remain intriguing proteins. Despite GarA and OdhI characterizations, their functions in bacteria are still elusive. The intrinsic property of the FHA domain, a phosphopeptide binding domain, is to link the protein to the phosphoregulation pathway. New features of their properties emerge, like their ability to bind nonphosphorylated peptides. This is the case for the GarA protein, that possesses the ability to bind its own phosphorylated N-terminal but also to nonphosphorylated protein. If the different binding modes have yet to be characterized in terms of affinity, the ability of the FHA-domain to bind to either phosphorylated or nonphosphorylated peptides using the same binding site is still biologically efficient. Moreover, in *M. tuberculosis*, their belonging to the phosphoregulation pathway is emphasized by the fact that the five FHA-containing proteins are STPKs substrates.

In previous studies, we measured substrate/STPK interactions. For instance, using fluorescence anisotropy, we measured an 8 μM Kd between Rv2175c and PknL (Cohen-Gonsaud et al., 2009). Here, we measure a 100 to a 1000 better affinity between Rv0020c and PknB. While the experiments were only performed here on Rv0020c and PknB, the existence of phosphorylation patterns on other STPK juxtamembrane domains makes similar interactions possible for others substrate/kinase pairs. In fact, such a binding could mean that the recruitment of the FHA-containing substrates and as a consequence their phosphorylation is a priority for *M. tuberculosis*. Moreover, two phosphothreonine residues represent two independent binding sites for Rv0020c_FHA. While the two sites coexist, we demonstrated that the Rv0020c_FHA binds preferentially to the position centered on pThr294 and that phosphorylation at position pThr309 generates a weaker affinity. Thus, it remains difficult to speculate about the possible biological significance of this in vitro characterization. Nevertheless, from the different data collected in the present study, we could hypothesize that regulation of FHA-containing substrates could be modulated, not only by the autophosphorylation of the juxtamembrane, but also by the phosphorylation pattern. This pattern could be established by either STPKs or STPKs phosphatases present in *M. tuberculosis*.

The structures we determined, and, in particular, the structure of Rv0020c_Nter, could not bring clear information on the putative function of Rv0020c. The structural homology between HypA and Rv0020c_Nter appears to be an evolutionary relic, as the conservation is limited to the core of secondary structure and as the domain and residues linked to the metals binding function of HypA are not present in Rv0020c. Interestingly, the striking point concerning Rv0020c architecture corresponds to its high degree of flexibility, as not only the protein possesses a 300 aa unfolded central domain but also harbors on its N-terminal part an extra 30 aa highly flexible extension. In *M. tuberculosis* proteins, and STPKs substrates, in particular, this flexible extension was shown to be important for the protein function as demonstrated for Rv2175c and GarA. Moreover, identification of the Rv0020c partner(s) and elucidation of the functional role of this protein remains necessary to understand the function of such large unfolded portion within the protein, which surely plays an important role into the protein function.

## EXPERIMENTAL PROCEDURES

### Bacterial Strains and Growth Conditions

Strains used for cloning and expression of recombinant proteins were *Escherichia coli* DH5α (Invitrogen) and *E. coli* BL21(DE3)Star (Novagen). Strains were grown at 37°C in LB medium supplemented with 100 μg/ml ampicillin.

### Cloning, Expression, and Purification of Recombinant Rv0020c Proteins

The full-length *Rv0020c* gene was amplified by PCR using *M. tuberculosis* H37Rv chromosomal DNA as a template and a set of primers containing a NdeI and an NheI site (Table S1). The Rv0020c_Nter and Rv0020c_FHA domains of Rv0020c were amplified by PCR using *M. tuberculosis* H37Rv chromosomal DNA as a template and a set of primers containing a NdeI and BamHI, and a NdeI and NheI site, respectively (Table 1). The amplified products were then digested with the appropriate restriction enzymes and

**Table 1. NMR and Refinement Statistics**

| | Rv0020c_Nter | Rv0020c_FHA |
|---|---|---|
| NMR distance and dihedral constraints | | |
| Distance constraints | | |
| Total NOE | 1497 | 1296 |
| Intraresidue | 458 | 327 |
| Interresidue | | |
| Sequential ($\|i-j\|=1$) | 483 | 416 |
| Medium range ($\|i-j\|<4$) | 209 | 137 |
| Long range ($\|i-j\|>5$) | 347 | 416 |
| Intermolecular | | |
| Hydrogen bonds | 92 | 64 |
| Total dihedral angle restraints | | |
| $\phi$ | 93 | 76 |
| $\psi$ | 93 | 76 |
| Structure statistics | | |
| Violations (mean and standard deviation) | | |
| Maximum distance constraint violation (Å) | 0.19 ± 0.05 | 0.14 ± 0.03 |
| Maximum dihedral angle violation (°) | 2.56 ± 1.01 | 3.25 ± 0.50 |
| Deviations from idealized geometry | | |
| Bond lengths (Å) | 0.0106 ± 0.0003 | 0.012 ± 0.001 |
| Bond angles (°) | 1.1328 ± 0.0370 | 1.257 ± 0.033 |
| Impropers (°) | 1.3694 ± 0.0996 | 1.423 ± 0.103 |
| Ramachandran plot (%) | | |
| Most favored region | 87.0 | 85.8 |
| Additionally allowed region | 12.9 | 12.7 |
| Generously allowed region | 0.1 | 1.3 |
| Disallowed region | 0.0 | 0.2 |
| Average pairwise rmsd (Å) | Residues 37–122 | Residues 436–527 |
| Backbone | 1.09 ± 0.23 | 1.02 ± 0.22 |
| Heavy | 1.82 ± 0.24 | 1.66 ± 0.22 |

Pairwise rmsd was calculated among 30 refined structures.

ligated into the pET_Tev plasmid harboring a variant of the His-tag fusion vector pET-15b, which was modified to contain a tobacco etch virus (TEV) protease site to replace the thrombin site coding sequence. All plasmids were verified using DNA sequencing. Site-directed mutagenesis on Rv0020c phosphorylation site was carried out according to the Stratagene QuickChange XL site-directed mutagenesis manual. Primers used for mutagenesis are detailed in Table 1. Mutation of the phosphorylated threonine residue of Rv0020c was created by substitution of Thr116 with alanine. The presence of the desired mutations was confirmed by sequencing.

All constructs were expressed as Tev-protease cleavable His-fusions in *E. coli* BL21 (DE3) star competent cells (Invitrogen). Recombinant strains harboring the different constructs were used to inoculate a 2 liter flask containing 750 ml of L-broth supplemented with 100 μg/ml ampicillin. The culture was grown in an orbital incubator set at 37°C and 220 rpm, until the $A_{600}$ of the culture reached 0.6 and then IPTG was added at a final concentration of 0.2 mM in order to induce the expression of Rv0020c proteins. Growth of the cultures was continued for a further 3 hr at a lower temperature of 30°C, after which the cells were harvested by centrifugation (using a Beckman Coulter Avanti J-20 XP centrifuge equipped with a 10,500 rotor and set at 7°C and 8000 rpm). The cell pellet arising from the 750 ml of culture was resuspended, on ice, in 30 ml of buffer A (50 mM Tris-HCl [pH 8.5], 150 mM NaCl) and 50 μl of 10 mg/ml lysozyme was added to aid in digestion of the cells. Cell pellets were stored at −80°C until required. Cells were then lysed by sonication (2 s bursts for 5 min, at 60% amplitude, with a large parallel probe; Vibra cell 72405), after which cell debris and insoluble materials were removed by centrifugation (using a Beckman Coulter Avanti J-20 XP centrifuge equipped with a 25.50 rotor, set at 18,000 rpm, at 7°C). The supernatant arising from this step was filtered through a 0.22 μm PVDF filter (Millipore) and then loaded through a AKTA basic system into a Hitrap 1 ml IMAC HP column (Amersham Biosciences), equilibrated in buffer A and 4% of buffer B (50 ml of buffer A supplemented with 500 mM of imidazole). $Ni^{2+}$-agarose affinity chromatography was then carried out at room temperature, to purify the His-tagged recombinant protein. The column was washed with successive applications of buffer A and 4% of buffer B (approximately 30 ml in total) to remove all the impurities and then buffer B was increased over 20 ml to 100%, which was collected in fractions of 0.5 ml. Fractions containing the Rv0020c proteins were identified by SDS-PAGE, then pooled and concentrated, using a 5 K cutoff concentrator, to a final volume of 5 ml (using a Sigma laborzentrifugh 3K15 bioblock scientific centrifuge set at 7°C, 4000 × g). The concentrated protein was applied to a Hiprep 26/10 (Amersham Biosciences) desalting column equilibrated in buffer A, to remove the imidazole in order to increase protein stability. The first two 5 ml fractions eluted, corresponded to the protein and so were pooled (total volume 10 ml) and placed in a labeled 15 ml falcon tube. The solution was treated for 2 hr at room temperature with TEV protease (approximately 1 OD of TEV for 100 OD of protein), to digest and thereby remove the N-terminal His-tag from the protein. Finally, the 10 ml of protein was concentrated (as before) to a final volume of 2 ml and applied to a Superdex 75 26/60 (Amersham Biosciences) size exclusion column, equilibrated in buffer 20 mM Na-Phosphate (pH 6.2), 150 mM NaCl. This led to the removal of any remaining impurities and the tag. Again, fractions containing the Rv0020c protein were identified by SDS-PAGE and then pooled and stored at −20°C until required. This protocol was carried out for all the nonlabeled constructs of Rv0020c as well as for $^{15}N$ and $^{15}N$ -$^{13}C$-labeled Rv0020c constructs, except that the cultures were grown in a minimum media containing $^{15}NH_4Cl$ and $^{15}NH_4Cl/^{13}C6$ glucose as the sole nitrogen and carbon sources.

### Cloning, Expression, and Purification of Recombinant PknB Proteins

The kinase domain (1–279) or the kinase domain with the juxtamembrane domain (1–331) of PknB were amplified by PCR using *M. tuberculosis* H37Rv chromosomal DNA as a template and a set of primers containing a NdeI and a BamHI site (Table S1). The amplified products were then digested with the appropriate restriction enzymes and ligated into the pET15b-TEV vector. All plasmids were verified using DNA sequencing. *E. coli* BL21(DE3) Star cells were transformed with the pET15b-TEV vector derivatives expressing the various PknB domain proteins. Recombinant *E. coli* strains harboring the pET15b-TEV derivatives were used to inoculate 200 ml of LB medium supplemented with ampicillin and incubated at 37°C with shaking until A600 reached 0.5. Isopropyl 1-thio-β-D-galactopyranoside was then added at a final concentration of 0.5 mM, and growth was continued for an additional 5 hr period at 25°C. The cells were harvested by centrifugation at 6000 × g for 10 min, washed in 10 ml of buffer A (50 mM Tris-HCl [pH 7.5], 150 mM NaCl, 10% glycerol, 1 mM EDTA, 1 mM aprotinin) and centrifuged again under the same conditions. The cell pellet was resuspended in buffer A. Cells were disrupted in a French pressure cell at 16,000 psi. The resulting suspension was centrifuged at 4°C for 30 min at 20,000 × g.

The supernatant was loaded through a AKTA basic system into a Hitrap 1 ml IMAC HP column (Amersham Biosciences), equilibrated in buffer A and 4% of buffer B (50 ml of buffer A supplemented with 500 mM of imidazole). $Ni^{2+}$-agarose affinity chromatography was then carried out at room temperature, to purify the His-tagged recombinant protein. The column was washed with successive applications of buffer A and 4% of buffer B (approximately 30 ml in total) to remove all the impurities and then buffer B was increased over 20 ml to 100%, which was collected in fractions of 0.5 ml. Fractions containing the OdhI protein were identified by SDS-PAGE, then pooled and concentrated, using a 5 K cutoff concentrator, to a final volume of 5 ml. The concentrated protein was applied to a Superdex S75 16/10 (Amersham

Biosciences) column equilibrated in buffer C (40 mM Tris-HCl [pH 7.9], 200 mM NaCl, 0.2 mM DTT, 0.2 mM EDTA, 10% glycerol), and pure fractions were pooled.

### Fluorescence Anisotropy

Rv0020c_Nter was covalently labeled with Atto647N succinimidyl ester dye (Invitrogen). A 10-fold molar excess of the dye was added to a solution of protein in 0.1 M sodium phosphate (pH 7.2) buffer and the reaction was allowed to proceed at room temperature for 3 hr with continuous agitation. The reaction was stopped by adding 10% Tris-HCl 1 M, and the excess of free dye was removed on a PD-10 column. Steady-state fluorescence anisotropy binding titrations were carried out on a Tecan Saphire II microplate reader, using a 635 nm LED for excitation, and a monochromator set at 680 nm (bandwidth 20 nm) for emission.

Binding data were analyzed using the package BIOEQS (Royer et al., 1990), a program that allows the fitting of the binding isotherm in terms of dissociation constants implicit in the model of choice. The simultaneous set of nonlinear free energy equations associated with the model is solved numerically in terms of the concentrations of the individual species postulated to exist.

The model, which was employed to fit the binding profiles, corresponds to the case where two PknB proteins bind to Rv0020c_FHA. Uncertainties on the recovered parameters were obtained by repeating a complete minimization over a range of tested parameter values, allowing all other parameters to float. The reported errors represent the uncertainties at the 67% confidence limit (i.e., 1 standard deviation) taking into account the correlation between all the parameters in the fits.

### In Vitro Kinase Assays

In vitro phosphorylation by PknB was carried out for 30 min at 37°C in a reaction mixture (20 µl) containing buffer P (25 mM Tris-HCl [pH 7.0]; 1 mM DTT; 5 mM $MgCl_2$; 1 mM EDTA) with 200 µCi/ml [$\gamma$-$^{33}$P]ATP. Phosphorylation of Rv0020c by PknB derivatives was performed with 5 µg of Rv0020c in 20 µl of buffer P with 200 µCi/ml [$\gamma$-$^{33}$P]ATP and 500 ng of PknB derivatives for 30 min at 37°C. The reaction was stopped by addition of an equal volume of 2 × sample buffer and the mixture was heated at 100°C for 5 min. After electrophoresis, gels were soaked in 16% TCA for 10 min at 90°C, and dried. Radioactive proteins were visualized by autoradiography using direct exposure to films.

In vitro phosphorylation for NMR and mass spectrometry analysis was performed as described above except that [$\gamma$-$^{32}$P]ATP was replaced by 5 mM nonradioactive ATP and incubated overnight.

### Mass Spectrometry Analysis

Purified Rv0020c was subjected to in vitro phosphorylation as described above. Subsequent mass spectrometry analyses were performed as previously described (Fiuza et al., 2008).

### Solution Structure of Rv0020c_Nter and Rv0020c_Cter

All NMR experiments were generally carried out at 20°C on Bruker Avance III 700 ($^{1}$H-$^{15}$N double resonance experiments) or Avance III 500 ($^{1}$H-$^{13}$C-$^{15}$N triple-resonance experiments) spectrometer equipped with 5 mm z-gradient TCI cryoprobe, using the standard pulse sequences (Sattler et al., 1999). NMR samples consist on approximately 0.5 mM $^{15}$N- or $^{15}$N,$^{13}$C-labeled protein dissolved in 10 mM phosphate buffer, 100 mM NaCl (pH 6.8) with 5% $D_2O$ for the lock. $^{1}$H chemical shifts were directly referenced to the methyl resonance of DSS, while $^{13}$C and $^{15}$N chemical shifts were referenced indirectly to the absolute $^{15}$N/$^{1}$H or $^{13}$C/$^{1}$H frequency ratios. All NMR spectra were processed and analyzed with GIFA (Pons et al., 1996).

NOE cross-peaks identified on 3D [$^{1}$H,$^{15}$N] NOESY-HSQC were assigned through automated NMR structure calculations with CYANA 2.1 (Güntert, 2004). Backbone $\varphi$ and $\phi$ torsion angle constraints were obtained from a database search procedure on the basis of backbone ($^{15}$N, HN, $^{13}$C', $^{13}$C$\alpha$, H$\alpha$, $^{13}$C$\beta$) chemical shifts using the program TALOS (Cornilescu et al., 1999). Hydrogen bond restraints were derived using standard criteria on the basis of the amide $^{1}$H / $^{2}$H exchange experiments and NOE data. When identified, the hydrogen bond was enforced using the following restraints: ranges of 1.8–2.3 Å for d(N-H,O), and 2.7–3.3 Å for d(N,O). The final list of restraints, from which values redundant with the covalent geometry has been eliminated. The 30 best structures (based on the final target penalty function values) were minimized with CNS 1.2 according the RECOORD procedure (Nederveen et al., 2005) and analyzed with PROCHECK (Laskowski et al., 1993). The rmsds were calculated with MOLMOL (Koradi et al., 1996). All statistics are given in Table 1.

## ACCESSION NUMBERS

The structure coordinates for the N- and C-terminal domains have been deposited in the Protein Data Bank (www.rcsb.org/pdb/) as entries 2LC0 and 2LC1, respectively. The chemical shifts have been deposited in the BioMagResBank under the accession numbers BMRB-17585 and BMRB-17586.

## SUPPLEMENTAL INFORMATION

Supplemental Information includes nine figures and one table and can be found with this article online at doi:10.1016/j.str.2011.07.011.

## ACKNOWLEDGMENTS

NMR experiments were recorded and analyzed using the facilities of the Structural Biology platform IbiSA (C.B.S., Montpellier, France). We thank Dr. Gilles Labesse and the A.B.C.I.S. team (http://abcis.cbs.cnrs.fr) for their helpful discussions. We thank M. Becchi, I. Zanella-Cléon, and A. Cornut (IBCP, Lyon, France) for their excellent expertise and technical assistance in mass spectrometry analysis. This work was supported by the "Agence National de la Recherche" (grant JC07_203251 for M.C.-G., and ANR-09-MIEN-004 for J.L. and V.M.). We declare that we have no competing financial interests.

Received: April 11, 2011
Revised: June 20, 2011
Accepted: July 7, 2011
Published: October 11, 2011

## REFERENCES

Alber, T. (2009). Signaling mechanisms of the Mycobacterium tuberculosis receptor Ser/Thr protein kinases. Curr. Opin. Struct. Biol. *19*, 650–657.

Alderwick, L.J., Molle, V., Kremer, L., Cozzone, A.J., Dafforn, T.R., Besra, G.S., and Fütterer, K. (2006). Molecular structure of EmbR, a response element of Ser/Thr kinase signaling in Mycobacterium tuberculosis. Proc. Natl. Acad. Sci. USA *103*, 2558–2563.

Barthe, P., Roumestand, C., Canova, M.J., Kremer, L., Hurard, C., Molle, V., and Cohen-Gonsaud, M. (2009). Dynamic and structural characterization of a bacterial FHA protein reveals a new autoinhibition mechanism. Structure *17*, 568–578.

Callebaut, I., Labesse, G., Durand, P., Poupon, A., Canard, L., Chomilier, J., Henrissat, B., and Mornon, J.P. (1997). Deciphering protein sequence information through hydrophobic cluster analysis (HCA): current status and perspectives. Cell. Mol. Life Sci. *53*, 621–645.

Cohen-Gonsaud, M., Barthe, P., Canova, M.J., Stagier-Simon, C., Kremer, L., Roumestand, C., and Molle, V. (2009). The Mycobacterium tuberculosis Ser/Thr kinase substrate Rv2175c is a DNA-binding protein regulated by phosphorylation. J. Biol. Chem. *284*, 19290–19300.

Cornilescu, G., Delaglio, F., and Bax, A. (1999). Protein backbone angle restraints from searching a database for chemical shift and sequence homology. J. Biomol. NMR *13*, 289–302.

Curry, J.M., Whalan, R., Hunt, D.M., Gohil, K., Strom, M., Rickman, L., Colston, M.J., Smerdon, S.J., and Buxton, R.S. (2005). An ABC transporter containing a forkhead-associated domain interacts with a serine-threonine protein kinase and is required for growth of Mycobacterium tuberculosis in mice. Infect. Immun. *73*, 4471–4477.

Durán, R., Villarino, A., Bellinzoni, M., Wehenkel, A., Fernandez, P., Boitel, B., Cole, S.T., Alzari, P.M., and Cerveñansky, C. (2005). Conserved autophosphorylation pattern in activation loops and juxtamembrane regions of

Mycobacterium tuberculosis Ser/Thr protein kinases. Biochem. Biophys. Res. Commun. *333*, 858–867.

Fernandez, P., Saint-Joanis, B., Barilone, N., Jackson, M., Gicquel, B., Cole, S.T., and Alzari, P.M. (2006). The Ser/Thr protein kinase PknB is essential for sustaining mycobacterial growth. J. Bacteriol. *188*, 7778–7784.

Fiuza, M., Canova, M.J., Zanella-Cléon, I., Becchi, M., Cozzone, A.J., Mateos, L.M., Kremer, L., Gil, J.A., and Molle, V. (2008). From the characterization of the four serine/threonine protein kinases (PknA/B/G/L) of Corynebacterium glutamicum toward the role of PknA and PknB in cell division. J. Biol. Chem. *283*, 18099–18112.

Güntert, P. (2004). Automated NMR structure calculation with CYANA. Methods Mol. Biol. *278*, 353–378.

Gupta, M., Sajid, A., Arora, G., Tandon, V., and Singh, Y. (2009). Forkhead-associated domain-containing protein Rv0019c and polyketide-associated protein PapA5, from substrates of serine/threonine protein kinase PknB to interacting proteins of Mycobacterium tuberculosis. J. Biol. Chem. *284*, 34723–34734.

Holm, L., and Rosenström, P. (2010). Dali server: conservation mapping in 3D. Nucleic Acids Res. *38* (Web Server issue), W545–W549.

Huse, M., and Kuriyan, J. (2002). The conformational plasticity of protein kinases. Cell *109*, 275–282.

Koradi, R., Billeter, M., and Wuthrich, K. (1996). MOLMOL: a program for display and analysis of macromolecular structures. J. Mol. Graph *14*, 51–55, 29–32.

Krissinel, E., and Henrick, K. (2004). Secondary-structure matching (SSM), a new tool for fast protein structure alignment in three dimensions. Acta Crystallogr. D Biol. Crystallogr. *60*, 2256–2268.

Laskowski, R.A., Moss, D.S., and Thornton, J.M. (1993). Main-chain bond lengths and bond angles in protein structures. J. Mol. Biol. *231*, 1049–1067.

Mahajan, A., Yuan, C., Lee, H., Chen, E.S., Wu, P.Y., and Tsai, M.D. (2008). Structure and function of the phosphothreonine-specific FHA domain. Sci. Signal. *1*, re12.

Molle, V., and Kremer, L. (2010). Division and cell envelope regulation by Ser/Thr phosphorylation: Mycobacterium shows the way. Mol. Microbiol. *75*, 1064–1077.

Molle, V., Kremer, L., Girard-Blanc, C., Besra, G.S., Cozzone, A.J., and Prost, J.F. (2003). An FHA phosphoprotein recognition domain mediates protein EmbR phosphorylation by PknH, a Ser/Thr protein kinase from Mycobacterium tuberculosis. Biochemistry *42*, 15300–15309.

Molle, V., Soulat, D., Jault, J.M., Grangeasse, C., Cozzone, A.J., and Prost, J.F. (2004). Two FHA domains on an ABC transporter, Rv1747, mediate its phosphorylation by PknF, a Ser/Thr protein kinase from Mycobacterium tuberculosis. FEMS Microbiol. Lett. *234*, 215–223.

Nederveen, A.J., Doreleijers, J.F., Vranken, W., Miller, Z., Spronk, C.A., Nabuurs, S.B., Güntert, P., Livny, M., Markley, J.L., Nilges, M., et al. (2005). RECOORD: a recalculated coordinate database of 500+ proteins from the PDB using restraints from the BioMagResBank. Proteins *59*, 662–672.

Nott, T.J., Kelly, G., Stach, L., Li, J., Westcott, S., Patel, D., Hunt, D.M., Howell, S., Buxton, R.S., O'Hare, H.M., and Smerdon, S.J. (2009). An intramolecular switch regulates phosphoindependent FHA domain interactions in Mycobacterium tuberculosis. Sci. Signal. *2*, ra12.

O'Hare, H.M., Durán, R., Cerveñansky, C., Bellinzoni, M., Wehenkel, A.M., Pritsch, O., Obal, G., Baumgartner, J., Vialaret, J., Johnsson, K., and Alzari, P.M. (2008). Regulation of glutamate metabolism by protein kinases in mycobacteria. Mol. Microbiol. *70*, 1408–1423.

Pennell, S., Westcott, S., Ortiz-Lombardía, M., Patel, D., Li, J., Nott, T.J., Mohammed, D., Buxton, R.S., Yaffe, M.B., Verma, C., and Smerdon, S.J. (2010). Structural and functional analysis of phosphothreonine-dependent FHA domain interactions. Structure *18*, 1587–1595.

Pons, J.L., Malliavin, T.E., and Delsuc, M.A. (1996). Gifa V. 4: A complete package for NMR data set processing. J. Biomol. NMR *8*, 445–452.

Royer, C.A., Smith, W.R., and Beechem, J.M. (1990). Analysis of binding in macromolecular complexes: a generalized numerical approach. Anal. Biochem. *191*, 287–294.

Sattler, M., Schleucher, J., and Griesinger, C. (1999). Heteronuclear multidimensional NMR experiments for the structure determination of proteins in solution employing pulsed field gradients. Prog. Nucl. Magn. Reson. Spectrosc. *34*, 93–158.

Scheef, E.D., and Bourne, P.E. (2005). Structural evolution of the protein kinase-like superfamily. PLoS Comput. Biol. *1*, e49.

Xia, W., Li, H., Sze, K.H., and Sun, H. (2009). Structure of a nickel chaperone, HypA, from Helicobacter pylori reveals two distinct metal binding sites. J. Am. Chem. Soc. *131*, 10031–10040.

 